Engineering in Life Sciences

WILEY-VCH

Engineering in Life Sciences

RESEARCH ARTICLE OPEN ACCESS

Engineering Caffeic Acid O-Methyltransferase for Efficient De Novo Ferulic Acid Synthesis

Huai Qi Shang[1,2,3,4] | Qing Bo Yang[1,2,3] | Shan Qiang[1,2,3,5] | Rong Zheng[1,2,3] | Chao Qun Zhang[1,2,3] | Ching Yuan Hu[1,2,3,6] | Qi Hang Chen[1,2,3,7] | Yong Hong Meng[1,2,3]

[1]Engineering Research Center for High-Valued Utilization of Fruit Resources in Western China, Ministry of Education, Shaanxi Normal University, Xian, Shaanxi, P. R. China | [2]National Research & Development Center of Apple Processing Technology, Shaanxi Normal University, Xian, Shaanxi, P. R. China | [3]College of Food Engineering and Nutritional Science, Shaanxi Normal University, Xian, Shaanxi, P. R. China | [4]Xianyang Weicheng Mile School, Xianyang, P. R. China | [5]Xi'an Healthful Biotechnology Co., Ltd., Xian, P. R. China | [6]Department of Human Nutrition, Food and Animal Sciences, College of Tropical Agriculture and Human Resources, University of Hawaii at Manoa, Honolulu, Hawai'i, USA | [7]Science Center for Future Foods, School of Biotechnology, Jiangnan University, Wuxi, China

Correspondence: Shan Qiang (qiangshan167@163.com) | Yong Hong Meng (mengyonghong@snnu.edu.cn)

Received: 15 November 2024 | **Revised:** 13 February 2025 | **Accepted:** 7 March 2025

Funding: This research was supported by the Natural Science Foundation of China (NSFC) Project (grant no. 32172145) and the Key Research and Development Plan in Shaanxi Province (2024NC-YBXM-171).

Keywords: biosynthesis | caffeic acid O-methyltransferase | enzyme engineering | ferulic acid | metabolic engineering

ABSTRACT

Ferulic acid is a high-value chemical synthesized in plants. The ferulic acid biosynthesis is still affected by the insufficient methylation activity of caffeic acid O-methyltransferase (*COMT*). In this study, we engineered *COMT* from *Arabidopsis thaliana* to match caffeic acid, and the mutant *COMT*$^{N129V\text{-}H313A\text{-}F174L}$ showed 4.19-fold enhanced catalytic efficiency for degrading caffeic acid. Then, we constructed the de novo synthesis pathway of ferulic acid by introducing tyrosine ammonia lyase from *Flavobacterium johnsoniae* (*FjTAL*), 4-hydroxyphenylacetate 3-hydroxylase from *Escherichia coli* (*EcHpaBC*), and mutant *COMT*$^{N129V\text{-}H313A\text{-}F174L}$, and further increased tyrosine synthesis. Furthermore, we overexpressed two copies of *COMT*$^{N129V\text{-}H313A\text{-}F174L}$ and enhanced the supply of S-adenosyl-L-methionine (SAM) by expressed S-ribosylhomocysteine lyase (*luxS*) and 5′-methylthioadenosine/S-adenosylhomocysteine nucleosidase (*mtn*) to increase the production of ferulic acid. Finally, the production of ferulic acid reached 1260.37 mg/L in the shake-flask fermentation and 4377 mg/L using a 50 L bioreactor by the engineered FA-11. In conclusion, *COMT* enzyme engineering combined with global metabolic engineering effectively improved the production of ferulic acid and successfully obtained a fairly high level of ferulic acid production.

1 | Introduction

Phenylpropanoid acids, including ferulic acid, caffeic acid, *p*-coumaric acid, and cinnamic acid, are the key building blocks for lignin [1–3]. Notably, phenylpropanoid acids provide carbon skeletons for synthesizing aromatic compounds, such as aromatic aldehydes, rosmarinic acids, and flavonoids [4, 5]. Among these phenylpropanoid acids, ferulic acid possesses various biological properties, such as antioxidant, anti-inflammatory, anticancer, and antithrombotic, and is widely used in food, cosmetics, and pharmaceuticals. In addition, ferulic acid is employed to treat and prevent certain diseases, such as COVID-19 [6]. Ferulic acid

Huai Qi Shang and Qing Bo Yang contributed equally to this study.

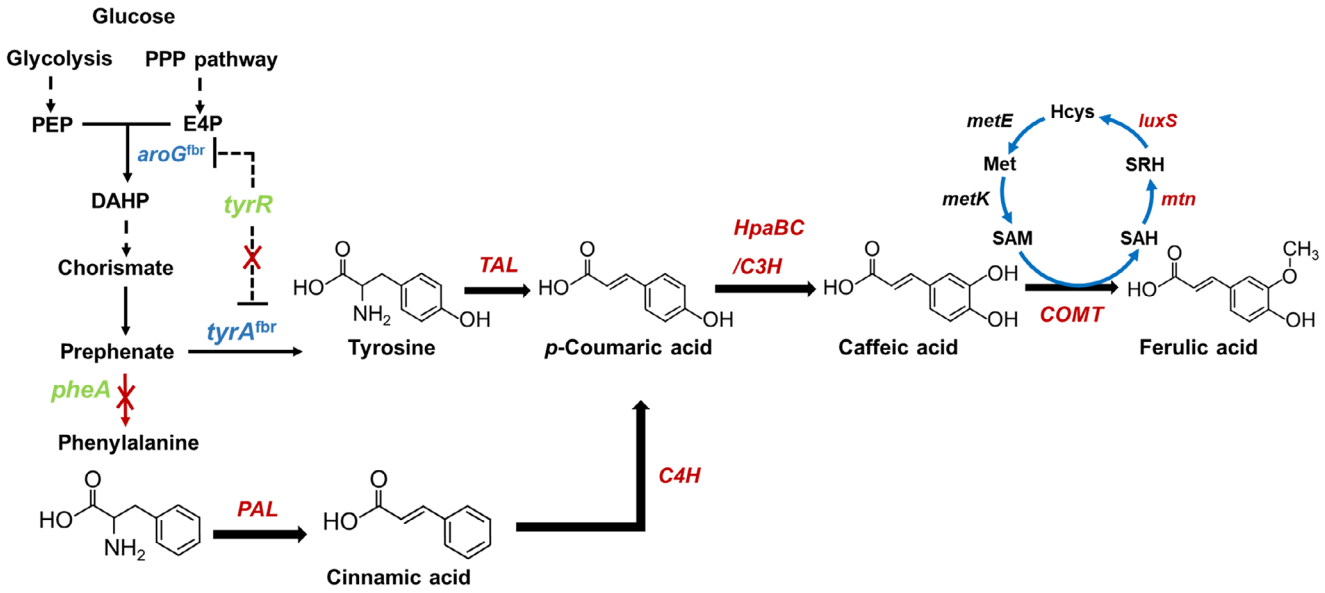

FIGURE 1 | De novo biosynthesis pathways of ferulic acid in *E. coli*. Green genes indicate gene knockouts; blue and red genes indicate overexpression. DAHP, 3-deoxy-D-arabinoheptulosonate 7-phosphate; PEP, phosphoenolpyruvate; PPP, Pentose phosphate pathway; E4P, D-erythrose 4-phosphate; SAM, S-adenosyl-L-methionine; SAH, S-adenosyl-L-homocysteine; SRH, S-ribosyl-L-homocysteine; Hcys, L-homocysteine; Met, methionine; *aroG*, 3-deoxy-7-phosphoheptulonate synthase; *tyrA*, chorismate mutase/prephenate dehydrogenase; *pheA*, prephenate dehydratase; *tyrR*, a regulatory protein; *TAL*, tyrosine ammonia lyase; *HpaBC*, 4-hydroxyphenylacetate 3-hydroxylase; *C3H*, *p*-coumarate 3-hydroxylase; *C4H*, *p*-coumarate 4-hydroxylase; *COMT*, caffeic acid O-methyltransferase; *PAL*, phenylalanine ammonia lyase; *mtn*, 5′-methylthioadenosine/S-adenosylhomocysteine nucleosidase; *luxS*, S-ribosylhomocysteine lyase; *metE*, methionine synthase; *metK*, methionine adenosyltransferase.

is also a precursor of many important compounds, including 4-vinylguaiacol, vanillin, and coniferyl alcohol [7–9]. Compared to extraction from plants and chemical synthesis, the microbial biosynthesis of ferulic acid has been widely studied because of its environment-friendly process and resource-conserving [8, 10].

Ferulic acid was produced mainly through the shikimic acid pathway from L-phenylalanine and L-tyrosine [11, 12]. These precursor amino acids were converted subsequentially to cinnamic acid and *p*-coumaric acid by phenylalanine ammonia lyase (PAL) and tyrosine ammonia lyase (TAL), respectively [13, 14]. The subsequent transformations, including hydroxylation or methylation of the benzene ring's C3-, C4-, and C5- sites, yielded an array of phenylacrylic acid derivatives [15]. Caffeic acid is a linchpin in the plant phenylpropanoid nexus. It was produced by converting *p*-coumaric acid by either *p*-coumarate 3-hydroxylase (C3H) or 4-hydroxyphenylacetate 3-hydroxylase (HpaBC) [16]. Finally, the C3'-OH of caffeic acid was methylated by caffeic acid O-methyltransferase (COMT) to produce ferulic acid (Figure 1) [17, 18]. *TAL*, *HpaBC*, and *COMT* were introduced into *Escherichia coli* and *Saccharomyces cerevisiae* to construct the metabolic pathways for de novo ferulic acid synthesis [19, 20]. The production of ferulic acid achieved the highest record of 5.09 g/L to date [8]. However, several limiting factors contributed to the low ferulic acid synthetic efficiency.

Hydroxylation and methylation of the benzene ring's carbon skeleton are bottlenecks of ferulic acid synthesis [8, 21]. In particular, *COMT* activity is a limiting factor for ferulic acid synthesis in the methylation step [16, 22]. *COMT* belongs to the S-adenosyl-L-methionine (SAM)-dependent O-methyltransferases (OMTs). *COMT* was attributed to the group-2 OMTs, which are typically 38–43 kDa proteins, metal ions independent, and catalyzes a range of compounds containing phenylpropanoid structures [16, 23]. The core structure of *COMT* from *Arabidopsis thaliana* (*AtCOMT*) consists of 21 α-helices and eight β-folds. It has three critical structural domains: the caffeic acid-binding domain, the S-adenosylmethionine-binding domain, and an auxiliary N-terminal domain [24]. Compared with the wild-type value of *MsCOMT* from *Medicago sativa*, the V_{max} to K_m-value of N131K increased 3.2-fold for caffeic acid by site-directed mutagenesis [25]. Structural analysis and targeted mutagenesis revealed the substrate-selective catalytic mechanism of *COMT* from *Ligusticum chuanxiong* (*LcCOMT*), especially, the I318T mutation increased the catalytic efficiency (K_{cat}/K_m) for methyl caffeate by 2.33-fold [23]. Therefore, the directed mutagenesis of *COMT*'s critical functional domain provides an essential strategy for improving catalytic activity. Recently, a high-throughput screening strategy was developed to enhance the catalytic efficiency of *AtCOMT* using a whole-cell biosensor. The best mutant V314R-A160S-H164N-F22Y-K111Y-S96C-V100D exhibited a 5.4-fold improvement in catalytic efficiency (K_{cat}/K_m) for caffeic acid [26]. Moreover, the methylation step is mediated by methyltransferases, with the cofactor SAM serving as the methyl donor. The SAM cycle was activated in *E. coli* by using endogenous S-ribosylhomocysteine lyase (LuxS) and 5′-methylthioadenosine/S-adenosylhomocysteine nucleosidase (Mtn) to supply sufficient methyl donor, and further improve the catalytic efficiency of *AtCOMT* [8]. Methionine as a direct precursor was used to increase the level of SAM, which was an effective strategy to enhance SAM and increased the production of vanillin by 32.68% [27]. Therefore, improving the enzymatic activity of *COMT* and the supply of intracellular SAM is key to improving the efficiency of ferulic acid synthesis.

In this study, to achieve the efficient biosynthesis of ferulic acid in *E. coli* BL21(DE3), the *COMT* was engineered to improve methylation efficiency and optimized a de novo biosynthesis pathway. In conclusion, *COMT* enzyme engineering combined with global metabolic engineering could effectively improve the production of ferulic acid. This study provided technical support and application basis for the industrial production of ferulic acid.

2 | Materials and Methods

2.1 | Strains and Media

All strains and plasmids used in this study are listed in Table S1. *E. coli* DH5α was used for plasmid construction and cultivated in a Luria−Bertani medium (LB) containing: 5 g/L yeast extract, 10 g/L peptone, and 10 g/L NaCl at 37°C, 200 rpm. *E. coli* BL21(DE3) was used to express heterologous genes and produce phenylpropanoid acids for ferulic acid synthesis. When needed, ampicillin, kanamycin, and isopropyl-beta-D-thiogalactopyranoside (IPTG) were added to the final concentration of 100 mg/L, 50 mg/L, and 0.2 mM, respectively. M9Y medium was used for de novo biosynthesis of ferulic acid [8].

The bioreactor fermentation was performed in a 50 L bioreactor (BLBIO-50SJA; Shanghai Bailun Biotechnology, Shanghai, China) containing 30 L fermentation medium [25 g/L glucose, 5 g/L yeast extract, 10 g/L peptone, 10 g/L $(NH_4)_2SO_4$, 2 g/L KH_2PO_4, 4 g/L Na_2HPO_4, 3 g/L $MgSO_4$, 0.1 g/L $CaCl_2$, 1.5 g/L sodium citrate dihydrate, 0.075 g/L VB1, and 1.5 mL of trace element solution]. Trace element solution contains the following: 2 g/L $Al_2(SO_4)_3{\cdot}18H_2O$, 0.75 g/L $CoSO_4{\cdot}7H_2O$, 2.5 g/L $CuSO_4{\cdot}5H_2O$, 0.5 g/L H_3BO_3, 24 g/L $MnSO_4{\cdot}H_2O$, 3 g/L $Na_2MoO_4{\cdot}2H_2O$, 2.5 g/L $NiSO_4{\cdot}6H_2O$, and 15 g/L $ZnSO_4{\cdot}7H_2O$). Five fresh colonies were inoculated in a shake flask containing 200 mL of LB medium with antibiotics and cultured at 37°C for 12 h. Then, the seed culture was inoculated in the bioreactor at 10% and cultured at 37°C. When OD_{600} reached around 15–20, 0.2 mM IPTG was added to induce protein expression, and then the temperature was adjusted to 30°C. The pH was maintained at 7.0. Glucose solution (75%) was added to keep the concentration constant (below 2 g/L). 20 g/L methionine was fed by the flow rate of 1 mL/h with a total volume of 100 mL. Oxygen was supplied in the form of filtered air via a sparging rate of 30–50 L/min of air using agitation in the 100–650 rpm range to maintain dissolved oxygen levels above 20%–30%.

2.2 | Plasmids and Strains Construction

Plasmid pET28a was used for the expression and purification of protein. Plasmids pETDuet-1 and pRSFDueT-1 were used to express multiple genes. Primers used in this study were synthesized by Sangon Biotech (Shanghai, China) and are listed in Table S2. The sequences of *TAL* (KR095307.1) from *Flavobacterium johnsoniae* (*FjTAL*) and *COMT* (AY062837.1) from *Arabidopsis thaliana* (*AtCOMT*) were synthesized by GenScript (Nanjing, China) with codon optimization and cloned into the pET28a-1. *FjTAL* and *AtCOMT* were inserted at the *Bam*HI/*Hind*III sites of pET28a-1 separately to form pET28a-*FjTAL* and pET28a-*AtCOMT*. pETDuet was linearized using primers pETDuet-F/pETDuet-R. The gene *EcHpaBC* from *E. coli* BL21(DE3) was PCR-amplified from the genomic DNA of *E. coli* with primers *HpaBC*-F/*HpaBC*-R. Then *EcHpaBC* fragment was inserted into linearized pETDuet-1 to generate pETDuet-*EcHpaBC* using the Seamless Cloning and Assembly Kit (TransGen Biotech; Beijing, China). Linearized pETDuet-*EcHpaBC* was obtained by using primers *HpaBC-TAL*-F/*HpaBC-TAL*-R. *FjTAL* was amplified from pET28a-*FjTAL* using primers RBS-*TAL*-F/RBS-*TAL*-R. *FjTAL* fragment was inserted into linearized pETDuet-*EcHpaBC* to generate pETDuet-*EcHpaBC-FjTAL*. *AtCOMT* or mutated *COMT* fragment was amplified with primers *COMT*-F/*COMT*-R from pET28a-*COMT* or mutated pET28a-*COMT*. The fragment was inserted into the linearized pETDuet-*EcHpaBC-FjTAL* to generate pETDuet-*EcHpaBC-FjTAL-AtCOMT* or mutant. *tyrR* and *pheA* were deleted by the pCas/pTargetF two-plasmid gene editing system [28]. The detailed method can be found in the Supporting Information.

2.3 | *AtCOMT* Mutation Library Construction and High-Throughput Screening

The *AtCOMT* mutation library was constructed using a fast mutagenesis system from TransGen Biotech (Beijing, China). The primers used for residues 129, 174, and 313 of *COMT* saturation mutations are listed in Table S2. The 50 μL PCR reaction mixtures were comprised of 1 μL template, 1 μL each of forward and reverse primers, 25 μL of 2× *TransStart FastPfu* Fly PCR SuperMix, and 22 μL nuclease-free water. The PCR was conducted under the following steps: 98°C 5 min, then 30 cycles of 95°C 20 s, 63°C 20 s, 72°C 120 s, and a final 72°C 10 min. 50 μL PCR products were digested by DMT enzyme at 37°C for 1 h. Finally, the digested products were transformed into *E. coli* BL21(DE3) for constructing the *AtCOMT* mutation library. When fresh colonies grow, forty single colonies were selected for auto-induced culture in 48-well plates. Three non-mutated *AtCOMT* single colonies were also set up as controls. After 24 h of auto-induced expression, 100 μL of 10 mM caffeic acid (final concentration 0.5 mM) was added to each well and incubated at 30°C with shaking at 200 rpm for 1.5 h. Then, 100 μL of the culture was taken, and 100 μL of methanol was added. The mixture was vortexed thoroughly and centrifuged at 12,000 rpm for 3 min. The supernatant was collected, filtered through a membrane (0.22 μm), and analyzed by HPLC (Agilent Technologies 1260 Infinity Series System, CA, USA).

2.4 | Molecular Modeling, Autodocking, and Molecular Simulation Methods

AtCOMT structural model was constructed as a monomer using SWISS-MODEL prediction (https://swissmodel.expasy.org/). The 3D molecule of caffeic acid was obtained by Chem 3D (version 20.0) and docked with the optimized *AtCOMT* model using AutoDock 4.2.6. Docking poses were visualized with PyMOL (version 2.5.4, Schrödinger, LLC). Molecular simulation was performed by Chen et al. [29] with minor modifications. A 100 ns molecular dynamics simulation was applied for each protein−ligand group with the GROMACS 2021.5 package and periodic boundary conditions. The Nose−Hoover thermostat cou-

pling methods were used to maintain the system temperature at 298 K. Moreover, snapshots of simulation results were visualized by VMD software.

2.5 | Metabolites Analysis

Chemical standards L-tyrosine, *p*-coumaric acid, caffeic acid, and ferulic acid were purchased from Macklin Reagent (Shanghai, China). Tyrosine, *p*-coumaric acid, caffeic acid, and ferulic acid were measured by HPLC-DAD. The column was C18 (Agilent Poroshell 120 EC-C18, 1.9 μm, 2.1 × 50 mm, 699675-902, USJSA03892, B19249). Compounds were separated by 0.5% phosphoric acid aqueous solution (Mobile Phase A) and acetonitrile (Mobile Phase B) at a flow rate of 0.8 mL/min under the following conditions: 90%–80% solvent A for 10 min, 80%–40% solvent A for 10 min, 40%–10% solvent A for 2 min, and 10%–90% solvent A for 3 min. Column temperature was set as 40°C. Tyrosine and phenylpropanoid acids were identified via matching retention time and UV spectrum with authentic standards (274 nm for tyrosine, 320 nm for *p*-coumaric acid, caffeic acid, and ferulic acid). The compounds were quantified based on calibration curves of various concentrations of standards using peak area. The data shown in this study were generated from three independent experiments.

2.6 | Statistical Analysis

All data were expressed as Mean ± SD, and each value was the mean of three independent experiments. All data were analyzed by one-way analysis of variance (ANOVA), and significance was determined using the least significant difference (LSD).

3 | Results

3.1 | Biosynthesis of Ferulic Acid From Tyrosine

Ferulic acid was synthesized in three steps from tyrosine. Tyrosine was first converted to *p*-coumaric acid by tyrosine aminotransferase (TAL), then hydroxylated to caffeic acid by 4-hydroxyphenylacetate 3-hydroxylase (HpaBC), and finally caffeic acid was converted to ferulic acid by *COMT*. For the biosynthesis of ferulic acid in *E. coli* BL21(DE3), we performed the pathway of ferulic acid synthesis from tyrosine by adding tyrosine exogenously. We screened out three enzymes including *FjTAL* derived from *Flavobacterium johnsoniae*, endogenous *EcHpaBC* from *Escherichia coli*, and *AtCOMT* from *Arabidopsis thaliana* by searching literature and enzyme databases (Figure 1). We first determined the enzymatic properties of *FjTAL*, *EcHpaBC*, and *AtCOMT*, respectively. The optimal reaction temperatures of the purified *FjTAL*, *EcHpaBC*, and *AtCOMT* were 40°C, 30°C, and 30°C, and the optimal reaction pH was 8.0, 7.0, and 8.0, respectively (Figure 2A–C).

To synthesize ferulic acid from tyrosine, the three genes were ligated into the pETDuet-1 plasmid to obtain pETDuet-*EcHpaBC-FjTAL-AtCOMT*. The plasmid pETDuet-*EcHpaBC-FjTAL-AtCOMT* was transformed into *E. coli* BL21 (DE3) to construct a whole-cell catalytic system that catalyzed the synthesis of ferulic acid from tyrosine. This strain was named FA-0. The system was able to catalyze the synthesis of ferulic acid (34.12 mg/L) at 30°C and pH 8.0. We measured the titer of *p*-coumaric acid, caffeic acid, and ferulic acid during the 12 h fermentation (Figure 2D). After 12 h of fermentation, *p*-coumaric acid was almost completely consumed, and caffeic acid accumulated at a high level. Therefore, the *COMT* reaction seemed to be the main bottleneck in the synthesis of ferulic acid. Moreover, the catalytic efficiency value (K_{cat}/K_m) of *AtCOMT* (28.93 $mM^{-1}min^{-1}$) was significantly lower than that of *FjTAL* (215.67 $mM^{-1}min^{-1}$) and *EcHpaBC* (174.13 $mM^{-1}min^{-1}$), which limited the ferulic acid production (Table S3, Figure S1).

3.2 | Engineering *COMT* to Improve Ferulic Acid

The *AtCOMT* homology model was simulated using O-methyltransferase from *Fragaria ananassa* as a template (PDB accession code: 6i71) with 81.09% similarity to the Swiss Model. The docking results of *AtCOMT* and caffeic acid were divided into substrate channel and substrate-binding domain. Upon entering the slit, the substrate caffeic acid passed through an access channel formed by residues L125, N129, M178, H313, and I317 (Figure 3A), creating a narrow aperture that imposed a site-blocking effect on the substrate. Therefore, we first site-directedly mutated the bulky residues at the five sites to shorter side-chain residues such as alanine, valine, and glycine. This expanded the space at the entrance of the substrate channel, thereby reducing the spatial site-blocking effect on the substrate. The L125 mutant was inactivated, while N129 and H313 exhibited higher catalytic activity (Figure 3B). Compared with the wild type, the accumulation of ferulic acid in N129V and H313A increased to 72.66% and 80.1%, respectively.

We further modified the *COMT* substrate-binding domain by saturation mutagenesis of five key residues (F161, H164, F174, W264, and N322), and selected representative mutants at each site for analysis. Most of the F161, H164, W264, and N322 mutants did not lead to an increase in ferulic acid production, but the F174 mutant led to a significant increase in ferulic acid production, with the accumulation of ferulic acid increasing to 103.8%. *AtCOMT* residue F174, the best mutant of ferulic acid was determined to be leucine (Figure 3C). Therefore, allowing the substrate to enter the substrate channel and interact with 174 was a key point to improve the catalytic activity of the enzyme. Through high-throughput screening, the optimal mutants N129V, H313A, and F174L were screened out.

In order to obtain mutants with higher activity, we assembled the above beneficial sites to obtain combined mutants. First, the two beneficial mutation sites N129V and H313A at the substrate channel were assembled to obtain mutant $COMT^{N129V\text{-}H313A}$, which increased the ferulic acid accumulation by 125.2%. Then, F174L was further assembled to obtain mutant $COMT^{N129V\text{-}H313A\text{-}F174L}$, which showed higher catalytic activity and increased the ferulic acid accumulation by 191.3% (Figure 3D). The optimal catalytic physicochemical conditions of the mutant $COMT^{N129V\text{-}H313A\text{-}F174L}$ were determined as 35°C and pH 8.0 (Figure S3). Compared with the wild-type *COMT*, the optimal temperature of the mutant $COMT^{N129V\text{-}H313A\text{-}F174L}$ was higher.

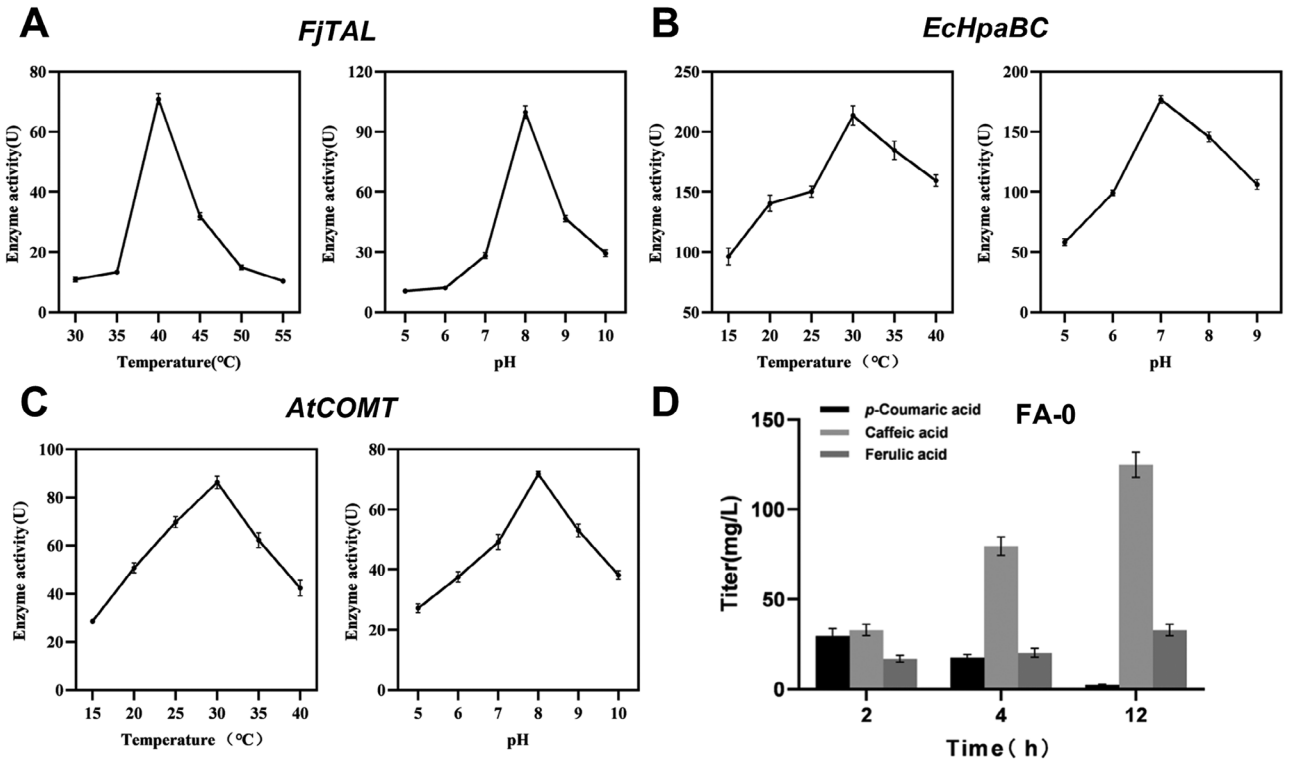

FIGURE 2 | Characterization of the enzymes for the synthesis of ferulic acid from tyrosine. (A) Effects of temperature and pH on *FjTAL* activity. (B) Effects of temperature and pH on *EcHpaBC* activity. (C) Effects of temperature and pH on *AtCOMT* activity. (D) Titers of *p*-coumaric acid, caffeic acid, and ferulic acid in strain FA-0 after 12 h of fermentation. Error bars represent standard deviations ($n = 3$).

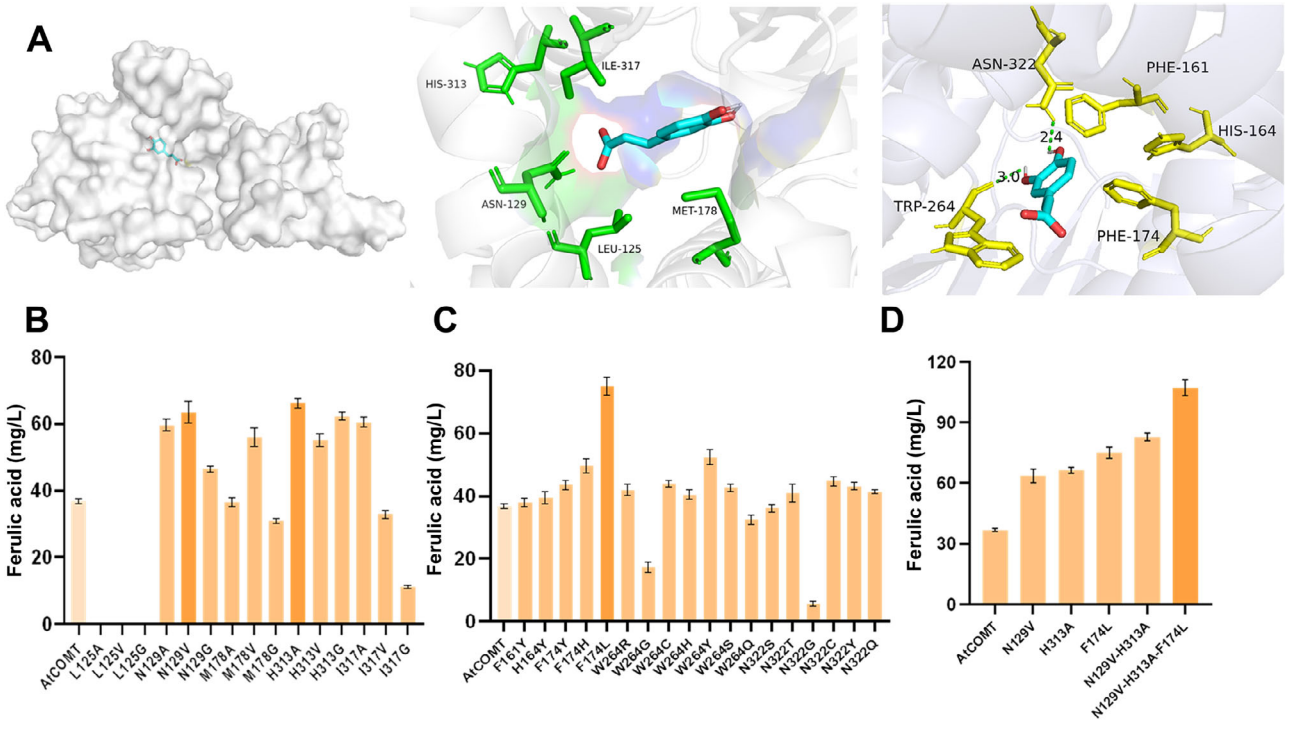

FIGURE 3 | Protein engineering of *AtCOMT*. (A) Determination of substrate channel and substrate-binding domain for *AtCOMT* by Auto Dock. (B) Site-directed mutagenesis of key residues in the substrate channel for ferulic acid titer. (C) Saturation mutagenesis of key residues in the substrate-binding domain for ferulic acid titer. (D) Beneficial mutated assembled *AtCOMT* for ferulic acid titer. Error bars represent standard deviations ($n = 3$).

TABLE 1 | Kinetic parameters of nonmutated and beneficial mutated assembled *AtCOMT*.

AtCOMT	K_m(mM)	K_{cat}(min^{-1})	K_{cat}/k_m($mM^{-1}min^{-1}$)	Fold
WT	0.67	19.59	28.93	—
AtCOMT^{N129V}	0.55	27.47	49.65	1.72
AtCOMT^{H313A}	0.65	23.98	36.37	1.26
AtCOMT^{F174L}	0.33	22.13	67.18	2.32
AtCOMT$^{N129V-H313A}$	0.35	29.86	83.32	2.88
AtCOMT$^{N129V-H313A-F174L}$	0.24	28.51	121.30	4.19

The kinetic parameters of *COMT* mutants were determined under optimal physicochemical conditions, and the catalytic efficiency of the mutants was compared with that of wild-type *COMT*. Mutations of different residues increased the substrate affinity and reaction rate of *COMT* to varying degrees. The catalytic efficiency (K_{cat}/K_m) of the five *COMT* mutants (N129V, H313A, F174L, N129V-H313A, and N129V-H313A-F174L) was 1.72-, 1.26-, 2.32-, 2.88-, and 4.19-fold higher than that of wild-type *COMT*, respectively (Table 1, Figure S4). Substrate channel and substrate-binding domain assembly at beneficial mutation sites increased substrate affinity and catalytic rate.

3.3 | Mechanism of Mutated *COMT* Catalytic Efficiency Improvement

To elucidate the mechanism of the high activity of *COMT*$^{N129V-H313A-F174L}$, the substrate-binding domains modified for substrate were analyzed in depth by molecular docking and MD simulation. Molecular docking of mutant *AtCOMT*$^{N129V-H313A-F174L}$ with the substrate caffeic acid and comparison with the molecular docking model of WT-*AtCOMT* with caffeic acid (Figure 4A). The results showed that the mutant *AtCOMT*$^{N129V-H313A-F174L}$ has a larger substrate channel compared to WT-*AtCOMT*, which reduced the spatial site resistance to the substrate and facilitates the opening of the substrate channel. Thus, this facilitates the substrate to enter the catalytic center to participate in the reaction.

To analyze the structural stability of the *COMT* enzymes in the presence of *COMT*-CA and *COMT*$^{N129V-H313A-F174L}$-CA, molecular dynamics simulations were performed, which could inform their effect on the perturbation of protein structural integrity. During the 100 ns simulation of the dynamics (Figure 4B), the protein and ligand reached relative equilibrium after 10 ns with a small range of fluctuations, indicating that the simulation results are reliable. Root means square deviation (RMSD) is used to measure the deviation change of the protein from its initial conformation to the final position. Therefore, the stability of the protein can be determined by the RMSD value obtained during the simulations [30]. The results showed that the RMSD value of mutant *COMT*$^{N129V-H313A-F174L}$ was lower than that of *COMT*, indicating that the structure of *COMT*$^{N129V-H313A-F174L}$ was more stable.

Root mean square fluctuation (RMSF) indicates the flexibility and mobility of each amino acid during the simulation. A higher RMSF value indicates better flexibility during the MD simulation, and a lower RMSF value indicates better system stability. It was calculated based on the movement of each residue along the trajectory near the mean position, and could reflect the flexibility of a certain region of the protein during the MD simulation [31]. By extracting the RMSF (B-factor) value of the residue tracks, the results showed that in the mutant *COMT*$^{N129V-H313A-F174L}$, the area around the N129V and H313A showed relatively high B-factor values, indicating greater flexibility than WT-*AtCOMT* (Figure 4C). The increased flexibility promoted a caffeic acid radical movement in the substrate access channel, thereby increasing the rate of caffeic acid bound to *AtCOMT*'s active center. Additionally, the B-factor values for residues within the range of positions 150–175 showed an increasing trend, indicating that the F174L mutation enhances the flexibility of the surrounding residues. This increased flexibility can facilitate interactions between residues, thereby improving the conversion efficiency.

3.4 | De Novo Biosynthesis of Ferulic Acid

The de novo biosynthesis module of ferulic acid includes two modules: the ferulic acid synthesis module (*FjTAL*, *EcHpaBC*, and *AtCOMT*) and the tyrosine synthesis module (Figure 5A). The ferulic acid synthesis module has been achieved by adding the substrate tyrosine. To achieve the de novo biosynthesis of ferulic acid in *E. coli*, the production of tyrosine, which is the precursor of ferulic acid, needs to be increased. Previous studies showed that relieving the feedback inhibition of two key enzymes *aroG* and *tyrA* could increase the yield of tyrosine [8, 32]. Therefore, plasmids pRSF-*aroG*^{fbr}-*tyrA*^{fbr} and pETDuet-*FjTAL-EcHpaBC-AtCOMT* were co-transformed into *E. coli* BL21 (DE3) to obtain the basic strain FA-1. The ferulic acid production of FA-1 was 48.53 and 61.06 mg/L at 48 and 72 h of fermentation, respectively (Figure 5C). To improve the supply of tyrosine, we knocked out the transcriptional regulatory protein (*tyrR*) of tyrosine biosynthesis to obtain BL21△*tyrR* strain. Furthermore, we knocked out prephenate dehydratase (*pheA*) to avoid carbon flux to the synthesis of phenylalanine in the competing pathway, thereby improving tyrosine biosynthesis and obtaining BL21△*tyrR*△*pheA* strain. Then, the pRSF-*aroG*^{fbr}-*tyrA*^{fbr} and pETDuet-*FjTAL-EcHpaBC-AtCOMT* plasmids were co-transformed into BL21△*tyrR* and BL21△*tyrR*△*pheA* strains to obtain FA-2 and FA-3 (Figure 5B). The ferulic acid production of FA-2 was 150.23 and 197.12 mg/L at 48 and 72 h of fermentation, respectively. The ferulic acid production of FA-3 was 210.7 and 246.99 mg/L at 48 and 72 h of fermentation, respectively (Figure 5C). Compared with FA-1, the ferulic acid production

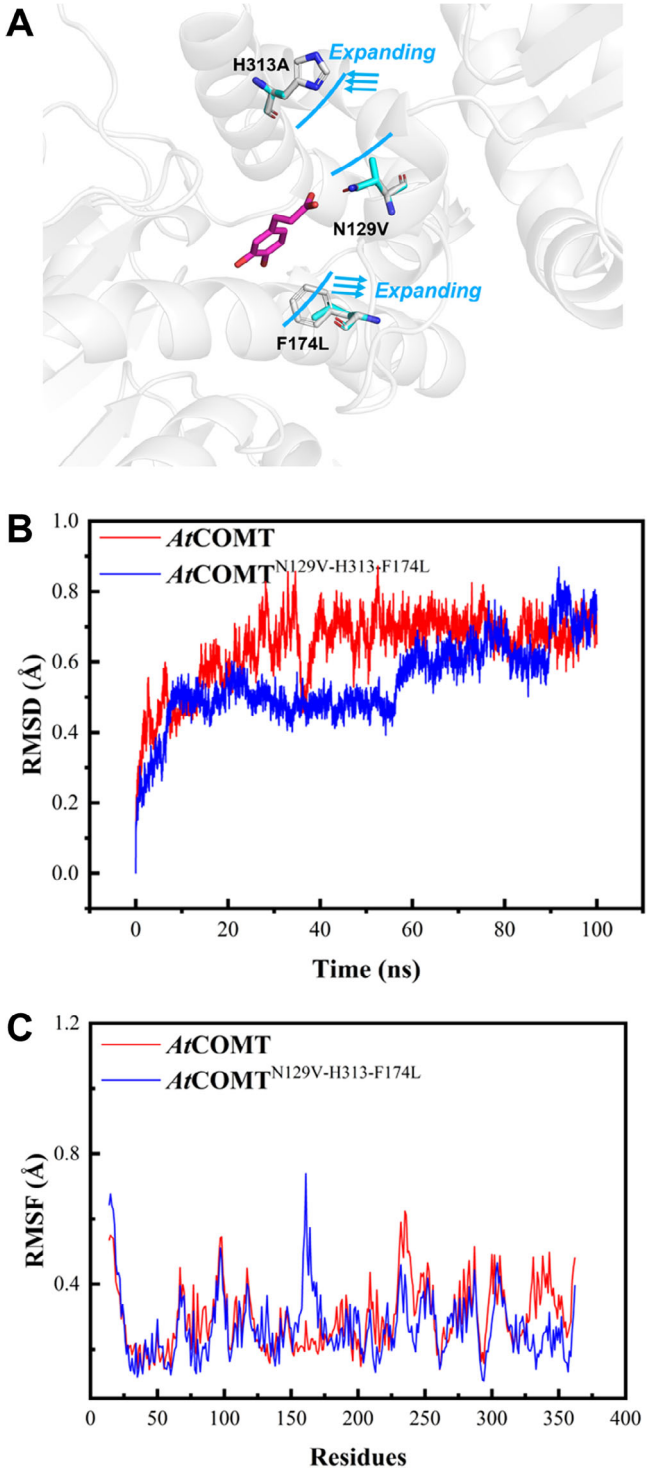

FIGURE 4 | (A) Autodocking for beneficial mutated assembled *COMT*$^{N129V\text{-}H313A\text{-}F174L}$ and caffeic acid. (B) Molecular dynamics simulation RMSD analysis. (C) Molecular dynamics simulation RMSF analysis. RMSD, root means square deviation; RMSF, root mean square fluctuation.

of FA-2 and FA-3 increased by 222.8% and 304.5% at 72 h of fermentation.

To improve the production of ferulic acid, we constructed mutant plasmids pETDuet-*EcHpaBC-FjTAL-AtCOMT*^{N129V}, pETDuet-*EcHpaBC-FjTAL-AtCOMT*^{H313A}, pETDuet-*EcHpaBC-FjTAL-AtCOMT*^{F174L}, pETDuet-*EcHpaBC-FjTAL-AtCOMT*$^{N129V\text{-}H313A}$, and pETDuet-*EcHpaBC-FjTAL-AtCOMT*$^{N129V\text{-}H313A\text{-}F174L}$. Then, these five mutant plasmids and pRSF-*aroG*^{fbr}-*tyrA*^{fbr} were co-transformed into BL21△*tyrR*△*pheA* strains to obtain FA-4, FA-5, FA-6, FA-7, and FA-8. The ferulic acid production of the five strains were 302.26, 303.80, 283.00, 420.71, and 552.76 mg/L at 72 h of fermentation, respectively (Figure 5D). Compared with FA-3, the ferulic acid production of the FA-4, FA-5, FA-6, FA-7, and FA-8 strains increased by 22.4%, 23%, 14.58%, 70.33%, and 123.79%, respectively. The construction of ferulic acid biosynthesis modules of FA-8 was shown in Figure 5B. The strain containing the *AtCOMT*$^{N129V\text{-}H313A\text{-}F174L}$ triple mutant gene had the highest ferulic acid production.

3.5 | Boosting *AtCOMT* Copy Number and SAM Supply for Ferulic Acid

Increasing the copy number of the rate-limiting gene can also effectively increase product production. Therefore, we increased the copy number of the key gene *AtCOMT* and constructed plasmids pRSF-*aroG*^{fbr}-*tyrA*^{fbr}-*AtCOMT*$^{N129V\text{-}H313A\text{-}F174L}$ and pRSF-*aroG*^{fbr}-*tyrA*^{fbr}-*AtCOMT*$^{N129V\text{-}H313A\text{-}F174L}$-*AtCOMT*$^{N129V\text{-}H313A\text{-}F174L}$. Plasmids pRSF-*aroG*^{fbr}-*tyrA*^{fbr}-*AtCOMT*$^{N129V\text{-}H313A\text{-}F174L}$ and pETDuet-*EcHpaBC-FjTAL-AtCOMT*$^{N129V\text{-}H313A\text{-}F174L}$ were co-transformed into BL21△*tyrR*△*pheA* strain to obtain the FA-9 containing two copies of the mutant *AtCOMT*$^{N129V\text{-}H313A\text{-}F174L}$ (Figure 5E). Plasmids pRSF-*aroG*^{fbr}-*tyrA*^{fbr}-*AtCOMT*$^{N129V\text{-}H313A\text{-}F174L}$-*AtCOMT*$^{N129V\text{-}H313A\text{-}F174L}$ and pETDuet-*EcHpaBC-FjTAL-AtCOMT*$^{N129V\text{-}H313A\text{-}F174L}$ were co-transformed into BL21△*tyrR*△*pheA* strain to obtain the FA-10 strain containing three copies of the mutant *AtCOMT*$^{N129V\text{-}H313A\text{-}F174L}$. The ferulic acid production of the FA-9 and FA-10 strains was 873.36 and 870.19 mg/L at 72 h of fermentation, respectively (Figure 5F). Compared with FA-8, the ferulic acid production of FA-9 and FA-10 increased by 57.99% and 57.43%, respectively. Therefore, we selected the FA-9 strain containing two copies of the mutant *AtCOMT*$^{N129V\text{-}H313A\text{-}F174L}$ for subsequent studies.

The intracellular cofactor SAM level is also a limiting factor for *COMT* gene methylation. To increase the SAM level, strategies such as adding methionine and constructing an endogenous SAM regeneration system in *E. coli* have been studied. The SAM cycle was activated in *E. coli* by overexpressing endogenous genes *luxS* and *mtn* to supply sufficient methyl donor [8]. Therefore, we overexpressed *luxS* and *mtn* in *E. coli* BL21(DE3) (Figure 1). As shown in Figure S4, BL21-AtC-LM overexpressing *luxS* and *mtn* could reach 916.2 mg/L of ferulic acid within 48 h, which is 71.1% higher than control BL21-AtC (535.5 mg/L) when fed with 1 g/L of caffeic acid. Subsequently, *luxS* and *mtn* were introduced into the ferulic acid synthesis pathway. The plasmid pRSF-*aroG*^{fbr}-*tyrA*^{fbr}-*AtCOMT*$^{N129V\text{-}H313A\text{-}F174L}$-LM was constructed, and then this plasmid and pETDuet-*EcHpaBC-FjTAL-AtCOMT*$^{N129V\text{-}H313A\text{-}F174L}$ were co-transformed into the BL21△*tyrR*△*pheA* strain to obtain the FA-11 (Figure 5E). The ferulic acid production of FA-11 was 1260.37 mg/L at 72 h of fermentation (Figure 5F). Compared with FA-9, the ferulic acid production of FA-11 increased by 44.31%, effectively increasing ferulic acid production.

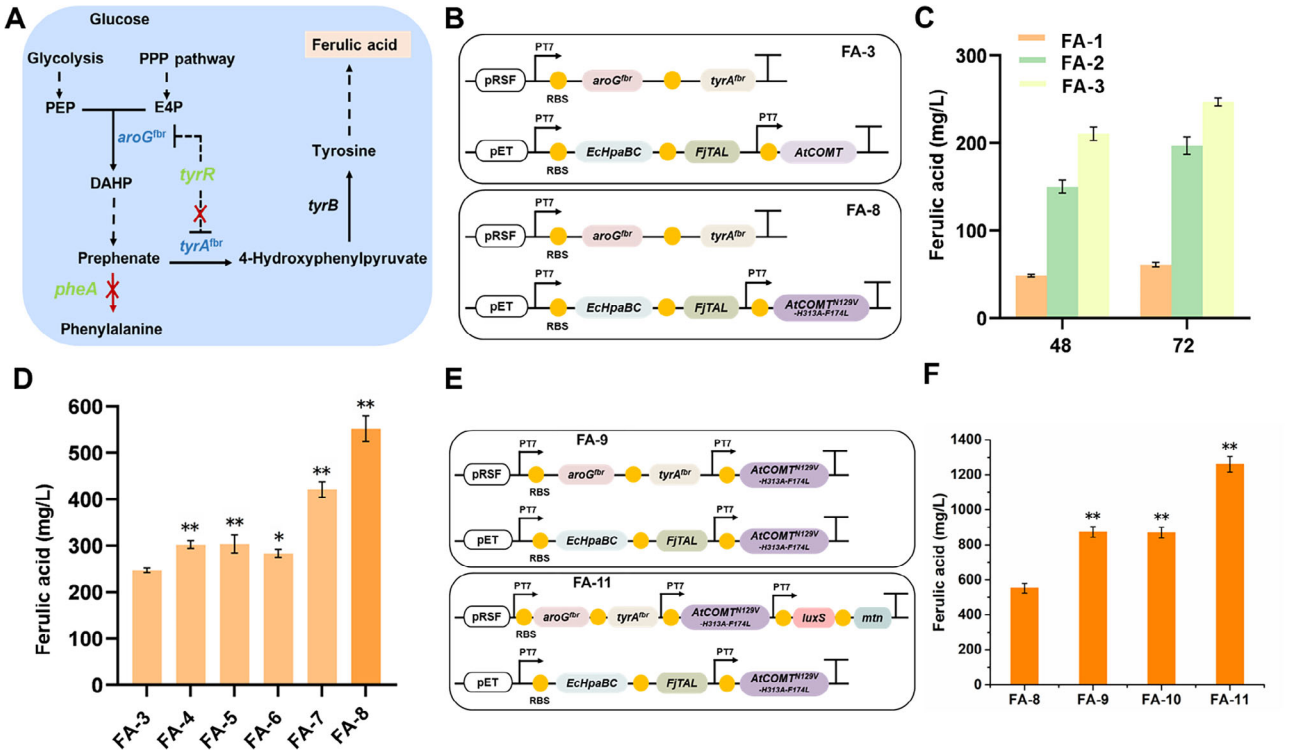

FIGURE 5 | Strategies for increasing ferulic acid production in *E. coli*. (A) Enhancement of the biosynthesis of precursor tyrosine through knocking out competing pathways and relieving feedback inhibition. (B) Construction of ferulic acid biosynthesis modules in FA-3 and FA-8 strains, respectively. (C) Effect of *tyrR* and *pheA* knockout on ferulic acid synthesis after 48 and 72 h of fermentation. (D) Expressed *COMT*, mutated $COMT^{N129V}$, $COMT^{H313A}$, $COMT^{F174L}$, $COMT^{N129V\text{-}H313A}$, and $COMT^{N129V\text{-}H313A\text{-}F174L}$ in FA-3, FA-4, FA-5, FA-6, FA-7, and FA-8 for ferulic acid titer after 72 h of fermentation, respectively. (E) Construction of ferulic acid biosynthesis modules in FA-9 and FA-11 strains, respectively. (F) Expressed mutated $COMT^{N129V\text{-}H313A\text{-}F174L}$, two copies of $COMT^{N129V\text{-}H313A\text{-}F174L}$, three copies of $COMT^{N129V\text{-}H313A\text{-}F174L}$, two copies of $COMT^{N129V\text{-}H313A\text{-}F174L}$, *luxS* and *mtn* in FA-8, FA-9, FA-10, and FA-11 strains for ferulic acid titer after 72 h of fermentation, respectively. Error bars represent standard deviations ($n = 3$). The asterisks indicate a significant difference compared with the control (*p <.05, **p <.01).

3.6 | Ferulic Acid Production in 50 L Bioreactor

To further investigate the ferulic acid accumulation characteristics of the engineered strain FA-11, the large-scale fermentation experiment was performed using a 50 L bioreactor with glucose as a carbon source. After the initial 25 g/L glucose was depleted, glucose was fed continuously into the medium to keep its concentration lower than 2 g/L. We considered the ferulic acid production without increasing for 6 h as the endpoint of fermentation. The fermentation experiment was repeated three times, and the results showed that the fermentation was reproducible. We chose one of the fermentation experiments for further analysis. The strain FA-11 began to accumulate ferulic acid at 18 h, and the ferulic acid production reached a maximum of 4377.4 mg/L at 66 h (Figure 6). The production of the intermediate product caffeic acid first increased and then decreased, reaching 284.6 mg/L at 72 h. The results showed that FA-11 can effectively produce ferulic acid.

4 | Discussion

COMT is a key enzyme in the plant phenylpropanoids pathway, which is involved in the biosynthesis of industrial and medical's molecules, such as flavonoids, anthocyanins, proanthocyanidins, and lignin [33–35]. In the de novo biosynthesis of ferulic acid, *COMT* is the last step in the synthesis, catalyzing the methylation of caffeic acid at the C3'-OH to produce ferulic acid. In this study, we engineered the substrate channel and substrate-binding domain of *AtCOMT* to facilitate substrate molecule entry and enhance the catalytic center to obtain higher activity.

Reconstructing the substrate channel is an effective approach to improve substrate delivery efficiency and enhance enzyme activity. Expanding the enzyme substrate channel can enhance enzyme activity. Mutating nonpolar hydrophobic residues near the substrate channel to smaller residues, such as N556A, could increase enzyme activity by 2.99-fold [36]. Alanine and valine are chiral amino acids with shorter side chains and reduced steric hindrance. When amino acid residues at the entrance of the substrate channel are mutated to those with shorter side chains, the channel entrance may be widened. The reduced steric hindrance of the side chains lowers the barrier for substrate entry, facilitating easier access. We created a loose hydrophobic channel at the entrance of the substrate channel using N129V and H313A mutations, which promoted substrate transfer and recognition. The catalytic efficiency of $AtCOMT^{N129V\text{-}H313A}$ was 2.88-fold that of wild-type *COMT*. Additionally, MD simulations of both $AtCOMT^{N129V\text{-}H313A}$ and wild-type *COMT* showed that the substrate access channel in $AtCOMT^{N129V\text{-}H313A}$ exhibited higher B-factor value fluctuations compared to the wild-type. Similar structural modifications have been reported in other

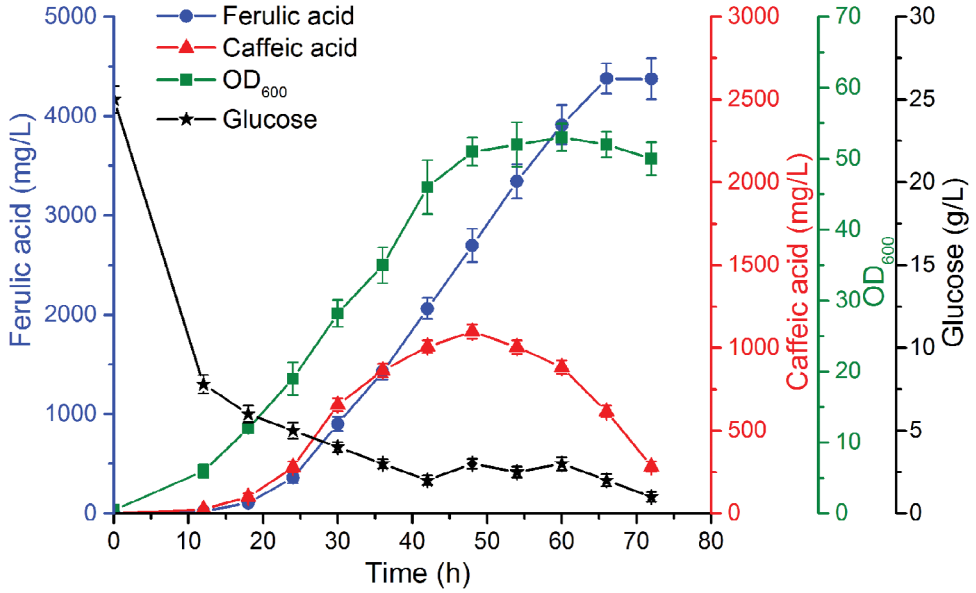

FIGURE 6 | Fermentation curves of ferulic acid production, caffeic acid production, OD600, and glucose in FA-11 using a 50L bioreactor. Error bars represent standard deviations ($n = 3$).

O-methyltransferases, where increasing the substrate channel resulted in higher catalytic efficiency [16]. Therefore, expanding the internal substrate channel to achieve higher conversion rates is one of the most effective strategies in enzyme engineering. In substrate-binding domain engineering, the F174L mutation plays a critical role in optimizing the substrate-binding domain by replacing the rigid phenylalanine residue with a more flexible leucine. In wild-type *AtCOMT*, phenylalanine imposed steric constraints that limit the efficient binding of caffeic acid. The F174L mutation provided additional space for the substrate, allowing it to interact more effectively with the enzyme during the catalytic process, thereby enhancing enzyme activity. As a result, the catalytic efficiency of *AtCOMT*$^{N129V\text{-}H313A\text{-}F174L}$ was 4.19-fold that of the wild-type *COMT*. In other methyltransferases, enhancing substrate channel flexibility and catalytic center stability could improve enzyme activity [37, 38]. Engineering both the substrate channel and the substrate-binding domain enhances substrate recognition, transfer, and binding, leading to higher enzyme activity. Through site-saturation mutagenesis in the substrate-binding domain and multiple rounds of random mutagenesis library screening, the catalytic efficiency of the *AtCOMT* mutant 72B3 (V314R-A160S-H164N-F22Y-K111Y-S96C-V100D) was improved by 5.4-fold compared to the wild type [26]. This study focused on optimizing the substrate channel and substrate-binding domain of *AtCOMT*.

Incorporating enzyme engineering with metabolic engineering has emerged as an effective strategy to enhance target compounds production. In the de novo synthesis of ferulic acid in *E. coli*, ensuring an adequate supply of precursors is essential for the efficient synthesis of ferulic acid. In previous studies, in order to increase the flux of tyrosine, the *tyrR* and *pheA* genes were knocked out [8, 32]. *tyrR* encodes a transcriptional regulatory protein for tyrosine biosynthesis, and its transcription is regulated by feedback inhibition of the final product tyrosine. The deletion of *tyrR* in *E. coli* increased the production of tyrosine. The *pheA* and *tyrA* compete to use the substrate prephenate to synthesize phenylalanine and tyrosine, respectively. Blocking *pheA* causes more carbon flux to flow to tyrosine rather than phenylalanine. In addition, overexpression of *aroG*^{fbr} and *tyrA*^{fbr} and the release of feedback inhibition could also increase the yield of tyrosine. Therefore, in order to have an adequate supply of tyrosine in ferulic acid production, we constructed the FA-8 strain, and the ferulic acid content reached 552.76 mg/L. Furthermore, increasing the copy number of the key gene *AtCOMT* and enhancing the SAM supply could also boost ferulic acid production [8]. Finally, the production of ferulic acid reached 1260.37 mg/L in the shake-flask fermentation by the engineered FA-11. In conclusion, the semi-rational engineering of *AtCOMT*, combined with metabolic engineering efforts, holds great promise for the efficient de novo synthesis of ferulic acid.

In future studies, biosensor-based rapid high-throughput screening methods can be employed to further improve the catalytic efficiency of *COMT*, thereby enhancing the production of ferulic acid. By integrating dynamic metabolic flux optimization, such as further increasing SAM supply and optimizing fermentation conditions, the production level of ferulic acid can be further elevated.

5 | Conclusion

In this study, we successfully developed an efficient de novo synthesis pathway for ferulic acid in *E. coli* by engineering the *AtCOMT*, combined with global metabolic engineering approaches. This method effectively enhanced the catalytic efficiency of the enzyme and increased ferulic acid yield, achieving a production level of 4377 mg/L in a 50 L bioreactor. This research provided a new strategy for the biosynthesis of ferulic acid and laid a technical foundation for its industrial application.

Acknowledgments

The authors thank Huai Qi Shang and Qing Bo Yang for their contribution to the design of this study, Qing Bo Yang and Rong Zheng for their conducting the experiments, Shan Qiang, Chao Qun Zhang, Ching Yuan Hu, Qi Hang Chen, and Yong Hong Meng for their data analysis and finishing the manuscript. This research was supported by the Natural Science Foundation of China (NSFC) Project (grant no. 32172145) and the Key Research and Development Plan in Shaanxi Province (2024NC-YBXM-171).

Conflicts of Interest

Shan Qiang was employed by Xi'an Healthful Biotechnology Co., Ltd. The remaining authors declare no conflicts of interest.

Data Availability Statement

All datasets obtained from this study are included in the manuscript/Supporting Information.

References

1. N. Kumar and N. Goel, "Phenolic Acids: Natural Versatile Molecules With Promising Therapeutic Applications," *Biotechnology Reports* 24 (2019): e00370.

2. I. El Houari, W. Boerjan, and B. Vanholme, "Behind the Scenes: The Impact of Bioactive Phenylpropanoids on the Growth Phenotypes of Arabidopsis Lignin Mutants," *Frontiers in Plant Science* 12 (2021): 734070.

3. J. Wang, X. Shen, J. Rey, Q. Yuan, and Y. Yan, "Recent Advances in Microbial Production of Aromatic Natural Products and Their Derivatives," *Applied Microbiology and Biotechnology* 102 (2018): 47–61.

4. A. Sharma, B. Shahzad, A. Rehman, et al., "Response of Phenylpropanoid Pathway and the Role of Polyphenols in Plants Under Abiotic Stress," *Molecules (Basel, Switzerland)* 24 (2019): 2452.

5. W. T. Park, M. V. Arasu, N. A. Al-Dhabi, et al., "Yeast Extract and Silver Nitrate Induce the Expression of Phenylpropanoid Biosynthetic Genes and Accumulation of Rosmarinic Acid in *Agastache rugosa* Cell Culture," *Molecules (Basel, Switzerland)* 21 (2016): 426.

6. Q. Dong, Y. Tan, G. Tang, et al., "Neuroprotective Potentials of Ferulic Acid Against Intracerebral Hemorrhage COVID-19 Through Using Network Pharmacology Approach and Molecular Docking Analysis," *Current Research in Toxicology* 5 (2023): 100123.

7. H. Lv, Y. Zhang, J. Shao, H. Liu, and Y. Wang, "Ferulic Acid Production by Metabolically Engineered *Escherichia coli*," *Bioresources and Bioprocessing* 8 (2021): 1–12.

8. Z. Zhou, X. Zhang, J. Wu, et al., "Targeting Cofactors Regeneration in Methylation and Hydroxylation for High-Level Production of Ferulic Acid," *Metabolic Engineering* 73 (2022): 247–255.

9. E. G. Lee, S. H. Yoon, A. Das, et al., "Directing Vanillin Production From Ferulic Acid by Increased Acetyl-CoA Consumption in Recombinant *Escherichia coli*," *Biotechnology and Bioengineering* 102 (2009): 200–208.

10. S. S. W. Effendi and I.-S. Ng, "High-Value Ferulic Acid Biosynthesis Using Modular Design and Spent Coffee Ground in Engineered *Escherichia coli* Chassis," *Journal of Bioresource Technology* 384 (2023): 129262.

11. M. Li, X. Cui, L. Jin, M. Li, and J. Wei, "Bolting Reduces Ferulic Acid and Flavonoid Biosynthesis and Induces Root Lignification in *Angelica sinensis*," *Plant Physiology and Biochemistry* 170 (2022): 171–179.

12. G. B. Kougan, T. Tabopda, V. Kuete, and R. Verpoorte, "Simple Phenols, Phenolic Acids, and Related Esters From the Medicinal Plants of Africa," *Medicinal Plant Research in Africa* (2013): 225–249.

13. T. Vogt, "Phenylpropanoid Biosynthesis," *Molecular Plant* 3 (2010): 2–20.

14. H. R. El-Seedi, A. M. El-Said, S. A. Khalifa, et al., "Biosynthesis, Natural Sources, Dietary Intake, Pharmacokinetic Properties, and Biological Activities of Hydroxycinnamic Acids," *Journal of Agricultural and Food Chemistry* 60 (2012): 10877–10895.

15. J. L. Ferrer, M. Austin, C. Stewart Jr, and J. Noel, "Structure and Function of Enzymes Involved in the Biosynthesis of Phenylpropanoids," *Plant Physiology and Biochemistry* 46 (2008): 356–370.

16. X. Wu, M. Yuwen, Z. Pu, et al., "Engineering of Flavonoid 3′-O-Methyltransferase for Improved Biosynthesis of Chrysoeriol in *Escherichia coli*," *Applied Microbiology and Biotechnology* 107 (2023): 1663–1672.

17. J. L. Rodrigues, D. Gomes, and L. R. Rodrigues, "A Combinatorial Approach to Optimize the Production of Curcuminoids From Tyrosine in *Escherichia coli*," *Frontiers in Bioengineering and Biotechnology* 8 (2020): 59.

18. S. Wang, S. Zhang, A. Xiao, et al., "Metabolic Engineering of *Escherichia coli* for the Biosynthesis of Various Phenylpropanoid Derivatives," *Metabolic Engineering* 29 (2015): 153–159.

19. R. Chen, J. Gao, W. Yu, et al., "Engineering Cofactor Supply and Recycling to Drive Phenolic Acid Biosynthesis in Yeast," *Nature Chemical Biology* 18 (2022): 520–529.

20. O. Choi, C. Z. Wu, S. Y. Kang, et al., "Biosynthesis of Plant-Specific Phenylpropanoids by Construction of an Artificial Biosynthetic Pathway in *Escherichia coli*," *Journal of Industrial Microbiology and Biotechnology* 38 (2011): 1657–1665.

21. D. C. Marcato, C. M. Spagnol, H. R. N. Salgado, V. L. B. Isaac, and M. A. Corrêa, "New and Potential Properties, Characteristics, and Analytical Methods of Ferulic Acid: A Review," *Brazilian Journal of Pharmaceutical Sciences* 58 (2022): 21.

22. M. Dornheim, B. Moritz, and M. Pietzsch, "Ferulic Acid Synthesis in Engineered *E. coli* Is Limited by Methyl-Group Supply," *New Biotechnology* 44 (2018): S41.

23. S. Song, A. Chen, J. Zhu, et al., "Structure Basis of the Caffeic Acid O-Methyltransferase From *Ligusticum chuanxiong* to Understand Its Selective Mechanism," *International Journal of Biological Macromolecules* 194 (2022): 317–330.

24. C. P. Joshi and V. L. Chiang, "Conserved Sequence Motifs in Plant S-adenosyl-L-methionine-dependent Methyltransferases," *Plant Molecular Biology* 37 (1998): 663–674.

25. P. Kota, D. Guo, C. Zubieta, J. Noel, and R. A. J. P. Dixon, "O-Methylation of Benzaldehyde Derivatives by "Lignin Specific" Caffeic Acid 3-O-methyltransferase," *Phytochemistry* 65 (2004): 837–846.

26. Z. Zhen, L. Xiang, S. Li, et al., "Bioelectronics, Designing a Whole-Cell Biosensor Applicable for S-adenosyl-l-methionine-dependent Methyltransferases," *Biosensors and Bioelectronics* 268 (2025): 116904.

27. A. M. Kunjapur, J. C. Hyun, and K. L. Prather, "Deregulation of S-adenosylmethionine Biosynthesis and Regeneration Improves Methylation in the *E. coli* De Novo Vanillin Biosynthesis Pathway," *Microbial Cell Factories* 15 (2016): 1–17.

28. Y. Jiang, B. Chen, C. Duan, et al., "Multigene Editing in the *Escherichia coli* Genome via the CRISPR-Cas9 System," *Applied and Environmental Microbiology* 81 (2015): 2506–2514.

29. Q. Chen, Y. Jiang, Z. Kang, et al., "Engineering a Feruloyl–Coenzyme A Synthase for Bioconversion of Phenylpropanoid Acids Into High-Value Aromatic Aldehydes," *Journal of Agricultural and Food Chemistry* 70 (2022): 9948–9960.

30. M. T. Khan and S. I. Malik, "Structural Dynamics behind Variants in Pyrazinamidase and Pyrazinamide Resistance," *Journal of Biomolecular Structure and Dynamics* 38 (2020): 3003–3017.

31. Y. Boulaamane, I. Ahmad, H. Patel, et al., "Structural Exploration of Selected C6 and C7-Substituted Coumarin Isomers as Selective MAO-B Inhibitors," *Journal of Biomolecular Structure and Dynamics* 41 (2023): 2326–2340.

32. B. Kim, R. Binkley, H. U. Kim, and S. Y. Lee, "Metabolic Engineering of *Escherichia coli* for the Enhanced Production of L-Tyrosine," *Biotechnology and Bioengineering* 115 (2018): 2554–2564.

33. C. T. Do, B. Pollet, J. Thévenin, et al., "Both Caffeoyl Coenzyme A 3-O-methyltransferase 1 and Caffeic Acid O-Methyltransferase 1 Are Involved in Redundant Functions for Lignin, Flavonoids and Sinapoyl Malate Biosynthesis in *Arabidopsis*," *Planta* 226 (2007): 1117–1129.

34. L. K. Narnoliya, R. Rajakani, N. S. Sangwan, V. Gupta, and R. S. Sangwan, "Comparative Transcripts Profiling of Fruit Mesocarp and Endocarp Relevant to Secondary Metabolism by Suppression Subtractive Hybridization in *Azadirachta indica* (Neem)," *Molecular Biology Reports* 41 (2014): 3147–3162.

35. R. Vanholme, K. Morreel, C. Darrah, et al., "Metabolic Engineering of Novel Lignin in Biomass Crops," *New Phytologist* 196 (2012): 978–1000.

36. R. Zheng, Q. Chen, Q. Yang, et al., "Engineering a Carotenoid Cleavage Oxygenase for Coenzyme-Free Synthesis of Vanillin From Ferulic Acid," *Journal of Agricultural and Food Chemistry* 72 (2024):12209–12218.

37. W. Wang, S. Su, S. Wang, L. Ye, and H. Yu, "Significantly Improved Catalytic Efficiency of Caffeic Acid O-Methyltransferase Towards N-acetylserotonin by Strengthening Its Interactions With the Unnatural Substrate's Terminal Structure," *Enzyme and Microbial Technology* 125 (2019): 1–5.

38. S. Xu, Q. Wang, W. Zeng, et al., "Construction of a Heat-Inducible *Escherichia coli* Strain for Efficient De Novo Biosynthesis of L-tyrosine," *Journal of Process Biochemistry* 92 (2020): 85–92.

Supporting Information

Additional supporting information can be found online in the Supporting Information section.